Exploring room- and low-temperature performance of Bio-waste Derived Hard Carbon Material in Half and Full Na-Ion Batteries

Xiuyi Lin [a], Xiaoqiong Du [a], Pui Shing Tsui [a], Jianqiu Huang [a], Hong Tan [a,b], Biao Zhang [a,b] *

[a]Department of Applied Physics, The Hong Kong Polytechnic University, Hung Hom, Hong Kong, P.R. China.

[b]The Hong Kong Polytechnic University Shenzhen Research Institute, Shenzhen, P.R. China

*Email: biao.ap.zhang@polyu.edu.hk

Abstract

Being abundant in nature, biomass is the most attractive precursors for producing hard carbon (HC) anodes for Na-ion batteries. The complexity of precursor has discouraged the development of a benchmark in synthesizing biomass-derived HC. Using longan peel waste as a model material, a facile two-step thermal treatment is proposed to avoid the self-activation, resulting in the HC with appropriate surface area and pore size distribution. A reversible capacity of 309 mAh g^{-1} is delivered, with an initial Coulombic efficiency of 80%. As-prepared HC is further investigated at a temperature as low as -20 ^oC to shed insights into the low temperature behavior of Na-ion batteries for practical application. In /ex situ XRD and Raman spectroscopy are conducted, exhibiting a safe and reversible capacity of 250 mAh g^{-1} without Na plating at −20 °C for HC. The full cell consists of HC/Na$_{3.5}$V$_2$(PO$_4$)$_2$F$_3$ is also examined at different temperatures. An energy density of 310 Wh kg^{-1} with an average discharge potential of 3.62 V is achieved at 25 °C. Whereas the formation of unstable SEI at low temperature leads to the capacity fading of the full cell at −20 °C. This finding reports a low-cost and high energy density Na-ion battery, and unveil the critical challenge of using HC for the low-temperature application.

Introduction

The studies in Na-ion batteries (NIBs) can trace back to 1970s, and recently they have attracted renewed attention as feasible alternatives to Li-ion batteries (LIBs). Benefiting from the vast abundance of Na minerals and the capability of using aluminum current collector on the anode side, NIBs are expected to reduce the cost by 30% compared LIBs, making them promising candidates for stationary energy storage.[1–3] For operating outdoorsy, the power source is required to adapt to different climate such as harsh winter. Therefore, the electrode materials that are able to sustain low temperature is of immense significance prior to the practical application of NIBs.

As intercalation of Na in the graphitic structure is less favored than Li and K, hard carbon (HC) that consisting of disordered graphitic layers are the most common anode material for NIBs.[4,5] Instead of intercalation, Na ions could be either adsorbed on the isolated graphitic layers or filled into the nanopores in the HC. A capacity of 200-300 mAh g^{-1} would be achieved depending on the synthesis procedures and the raw materials adopted.[6] Being natural abundant and environmental friendly, biomass waste is widely studied as precursors for producing HC.[7–12] In general, the biomass is made up of various biopolymers, including hemicellulose, cellulose, lignin, pectin, protein, free sugar and so on. The ratio of them varies in the individual materials, giving rise to distinct electrochemical performance. A great number of works have been devoted to the screening of appropriate precursors, and several excellent candidates have been discovered such as banana peels[7] and corn cobs[11]. In addition to the precursors, the calcination protocol also plays a vital role in determining the microstructure of the final products. Nevertheless, there is absent of any benchmark on the sintering processes. A similar carbonization temperature range of 1000-1400 °C has been adopted, but the intermediate steps differs a lot in the previous works. It calls for a general guideline in designing the calcination protocol for efficiently developing biomass-derived HC.

The performance of HC has been extensively investigated at or above room temperature. Nevertheless, it has been reported with poor performance in the subzero range.[13–15] At low temperature, the polarization would lower the sodiation potential of hard carbon, i.e., form ~ 0.1 V to 0.02 V, a poor capacity is then obtained as sodiation is

incomplete at the cut-off voltage 0V. Furthermore, the low potential may trigger the Na plating, turning the benefit of low voltage plateau in hard carbon to the severe safety issues. In view of this, there are few studies for low temperature NIBs using hard carbon as the anode. Instead, more attention is attracted to the alloy or carbon/alloy composite for their adequate capacity of around 100 mAh g^{-1} at low temperatures, such as Ti-based metal oxides,[16,17], Se/graphene[18] and Sb/CNT[19] composites. However, these anode materials are accompanied by the high average voltage, which is detrimental to the energy density of the full cell. Previous work indicates that the capacity of hard carbon may be fully utilized by lowering the cut-off potential to below 0 V.[20] It indeed allows a high capacity of 265 mAh g^{-1} at -15 °C,[21] although the possibility of Na plating requires prudent investigation.

In this work, the calcination protocol of synthesizing HC from biomass waste is systematically explored. It shows a significant dependence of the performance on the heat treatment processes. The optimized HC was then evaluated at both the room and low-temperature. Assisted with the in situ and ex situ XRD, the possibility of Na metal plating is thoroughly examined. A safe and reversible capacity of 250 mAh g^{-1} at −20 °C for HC is obtained without Na plating in HC. Furthermore, a $Na_{3.5}V_2(PO_4)_2F_3$ cathode was prepared to couple with HC for investigating the low temperature behaviors of HC in full cell, which has been rarely studied.

Experiment

Materials

The HC material was prepared from longan peel as schematized in Figure 1a. The fresh longan peels were washed with hot DI water, 1 M HCl solution and DI water in sequence. The collected product is dried at 80 °C for 24 h. The dried longan peel was directly carbonized at 1350 °C under an argon atmosphere, and the obtained sample was denoted as L-1350. In the other path, dried materials are firstly pyrolyzed in a tubular furnace at 450 °C for 1 h under Argon gas, and the captured carbon was gridded (or washed) after cooling down, followed by heating at 1350 °C, the as-synthesized carbon is denoted as L-450-1350 (or L-450-wash-1350). Lastly, the L-450-1350 was rinsed with DI water to

remove the remaining impurities and dried at 60 °C for 12 h, and the product is denoted as L-450-1350-wash. For the cathode, the $Na_3V_2(PO_4)_2F_3$ (NVPF) was synthesized through a conventional sol-gel method.[22] The obtained NVPF powder was mixed with a stoichiometric amount of Na metal and ball-milled for 15 min using a Spex 8000M ball-miller to prepare $Na_{3.5}V_2(PO_4)_2F_3$ phase according to our previous work.[23]

Material characterization

X-ray diffraction (XRD) was conducted with a Rigaku SmartLab with a Cu Kα radiation source. The in situ and ex situ XRD patterns were recorded using Swagelok cell equipped with a beryllium window, which also severed as the current collector for HC. Particle morphologies were examined using a transmission electron microscope (TEM, JEOL 2010F) and scanning electron microscope (SEM, JEOL-6490). The Raman spectra were obtained using Witec Confocal Raman system with a 532nm laser. Nitrogen adsorption/desorption isotherms were measured to probe the surface area and porosity on a micromeritics ASAP 2020 machine.

Electrochemical measurements

Coin cells (CR2032) were used to test the electrochemical performances. 1M $NaClO_4$ solution in a mixture of ethylene carbonate/propylene carbonate (EC/PC) (1:1 in volume) was applied as the electrolyte for the half cell and full cells. Two pieces of Whatman glass fibers soaked with the electrolyte were used as the separator between the positive and negative electrode. The HC electrode was prepared by casting a slurry of 90 wt% HC, 5 wt% conductive carbon black and 5 wt% polyvinylidene fluoride (PVDF) binder on copper foil. In companions, electrodes using carboxymethylcellulose sodium salt (CMC) and sodium alginate (NaAg) as the binder were also prepared. Typical loading mass of the HC electrode was around 1.5 mg cm^{-2}. For the full cell, $Na_{3.5}V_2(PO_4)_2F_3$ powders were mixed with 20% carbon SP for the preparation of positive electrodes. The weight ratio of the positive/negative electrodes was 2.5. The cells were galvanostatic charged/discharged with a LAND 2001 CT battery test system (Wuhan, China) under various voltage ranges and

current rates. Electrochemical impedance spectroscopy (EIS) was carried out on a VMP system (Biologic S.A., Claix, France).

Results and Discussions

The preparation of biomass-derived HC usually involves washing for removing impurities, mechanical crush to reduce the size, and pyrolysis at temperatures between 600 °C and 1500 °C. The microstructure of HC would be significantly affected by the fabrication steps, but a general principle on designing the calcination protocol is absent. Thus, a longan peel waste is adopted as a precursor; the effect of pyrolysis strategies on the Na storage performance are probed. The synthesis process of HC from longan peel waste is schematized in Figure 1a. The fresh longan peel was washed to remove sugars, phenolic compounds, and pectic polysaccharides. The collected product mainly consists of cellulose (~67%) and lignin (~27%).[24] Both cellulose and lignin are highly cross-linked, discouraging the graphitization process and leading to a porous structure making up of randomly oriented graphitic layers.[8] Four samples were prepared through different approaches, and their XRD patterns are shown in Figure 1b. In all the spectra, broad (002) and (100) diffraction peaks at 22.1° and 43.6° are observed, indicating the characteristic of disordered carbon. The corresponding interlayer distance is calculated to be 0.4 nm, which is larger than that of graphite, facilitating the insertion and extraction of Na. Peaks from impurities (Na_2SO_4, $Na_2S_2O_3$, and NaS, etc.) are detected in all the samples except in L-450-1350-wash, while direct carbonization at 1350 °C (L-1350) gives the most significant amount. These impurities originate from the intrinsic structure of longan peel; hence they cannot be eliminated in the initial washing process but could be mostly removed as the decomposition product during the pre-pyrolysis at 450 °C. The following carbonization at 1350 °C still left a few residual impurities while it could be removed by washing the final product.

To explore the effect of the impurities on the carbonization, the porous structures of four HC samples were then characterized using N_2 adsorption/desorption measurements. The corresponding BET surface area and pore distribution are shown in Figure 1c and 1d. L-1350 displays a Type I isotherm curve similar to activated carbons, with a specific surface area of 268.1 m^2 g^{-1} and a large number of micropores within 10 Å. It seems that

the impurities are active in pore development at high temperature leading to the high surface area of L-1350 with the presence of micropores. XRD results show that intermediate calcination at 450 °C is helpful in removing the impurities, reducing the activation effects. Therefore, a much lower BET surface area of around 6 $m^2 g^{-1}$ is obtained in L-450-1350. It is noted that a washing step after 450 °C treatment has a marginal benefit on getting rid of the impurities. Hence a similar surface area is observed in L-450-wash-1350 — the pores of both samples located in the range of 300–2000 Å. Additional washing after carbonization at 1350 °C would remove the residual impurities as evidenced by XRD. Thus, L-450-1350-wash presents numerous pores in the range of 10-30 Å which were covered by contaminants in unwashed samples, resulting in a higher surface area of 32.6 $m^2 g^{-1}$. The morphology of as-prepared L-450-1350-wash is further confirmed by SEM and TEM. It shows an irregular shape with a large particle size in the range of 10-40 µm, and the washed sample shows a clean surface (Figure 1e and 1f). The TEM image in Figure 1g reveals the typical turbostratic graphitic microstructures, which presents a characteristic feature of hard carbon materials proposed by Dahn and co-workers.[25] No presence of long-range graphene layers is observed. Instead, 4-7 layers of short-range parallel carbon hexagonal layers are found, which are active sodium storage sites according to previous works.[26] In addition, the curved graphene layers formed some closed nanovoids, providing extra sodium storage sites through pore filling.

It is demonstrated here the importance of an intermediate calcination step at low temperature for avoiding the activation process. Biomass waste share similarities in the components although the exact composition differs. The protocol developed may also applicable to another biomass candidate. A green tea waste is adopted as an example; the same two-step thermal treatment approach was applied (Figure S1). A similar trend has been discovered. A high surface of 130.4 $m^2 g^{-1}$ is obtained with direct carbonization at 1350 °C, where considerable micropores are found. The value is substantially decreased to 32.4 $m^2 g^{-1}$ once an intermediate step at 450 °C is added. It is speculated that a pre-heat treatment is necessary before final carbonization for producing biomass waster derived HC with low surface area, particularly for those precursors contain carbonate-or sulfate- based impurities. The reason lies in the presence of the impurities may sever as self-activation agents to introduce micropores in the final product. These impurities cannot be removed

by washing even in the acid solution, but only possible with thermal decomposition under a medium temperature.
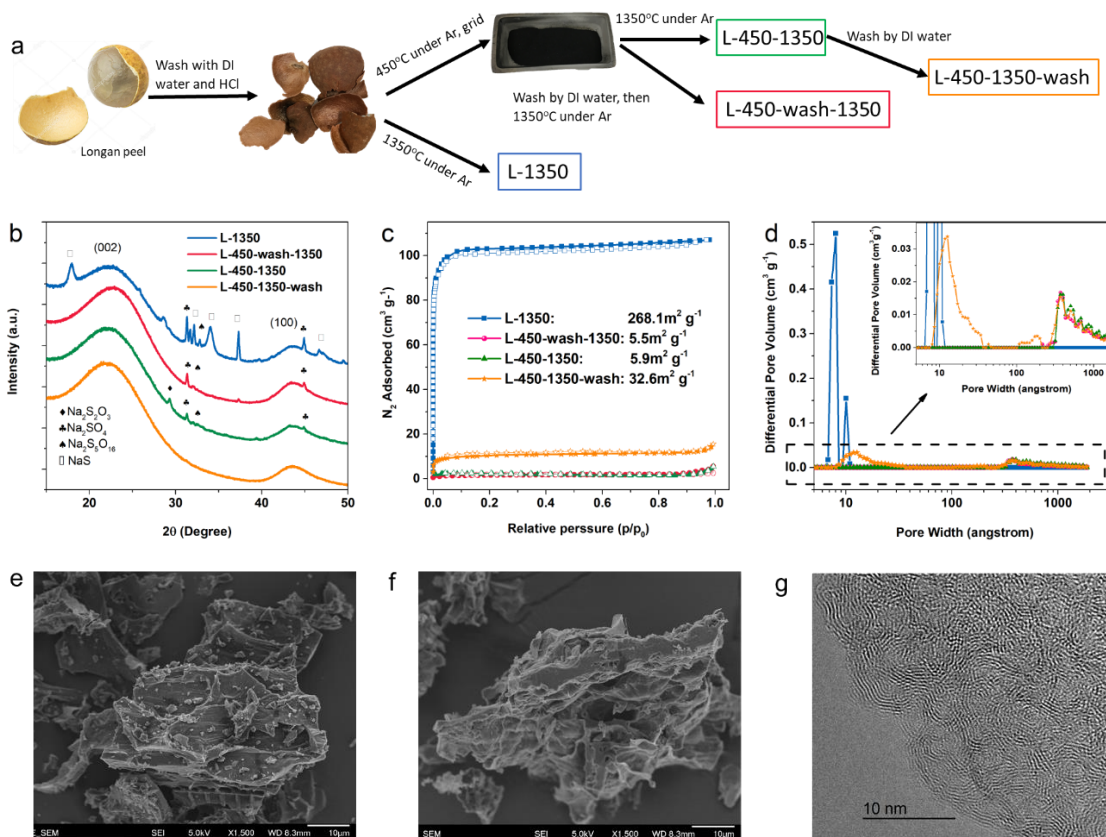

Figure 1 a) Schematic protocol used to obtain HC from longan peel. b) XRD, c) adsorption-desorption isotherms and d) DFT pore size distribution of longan samples prepared by different methods. SEM images of e) L-1350 and f) L-450-1350-wash. g) TEM images of L-450-1350-wash.

To explore the effect of the microstructure on the sodium storage performance, the samples were first characterized in half cells with metallic Na as the counter electrode. The voltage profiles of longan peel derived HC are shown in Figure 2a. Large irreversible capacity is found in L-1350 due to the high surface area, which gives rises to copious solid electrolyte interphase (SEI). The initial Coulombic efficiency is highly improved in the other three samples, which possess much lower surface area arising from the pre-treatment at 450 $^{\circ}$C. In particular, slightly higher capacity is obtained in L-450-1350-wash than the samples without a final wash step. Both the removal of the resident impurities and the

introduction of appropriate pores are beneficial to increasing the available capacities. The HC made from green tea waste also delivers a similar phenomenon, where a pre-heating increase both the initial Coulombic efficiency and reversible capacity (Figure S1b). It further confirms the importance of an intermediate calcination step for producing high-performance HC from bio-waste.

The following mechanism study focuses on optimized sample L-450-1350-wash. It will be simply denoted as HC for clear description. At a current density of 25 mA g^{-1}. The sample shows a first charge and discharge capacities of 383.6 and 309.3 mAh g^{-1} respectively, giving an initial coulombic efficiency of 80.7%. Majority of the capacity (~200 mAh g^{-1}) is received at the low voltage plateau region at around 0.1 V (all potentials in half-cell are vs. Na^{+}/Na). A reversible capacity of ca. 300 mAh g^{-1} is maintained in the following cycles as shown in the inset. The rate capability test in Figure 2b exhibits excellent stability at the current density below 100 mA g^{-1}. However, the capacity fast degrade when current density reaches 250 mA g^{-1}. It may attribute to the highly resistant SEI layer formed in carbonate electrolyte.[27] To fully demonstrate the rate performance, an ether-based electrolyte consisting of 1M NaBF$_4$ in diglyme is adopted. As shown in Figure 2b, similar capacities are achieved in diglyme electrolyte at the small rates, while capacities are much higher at the large rates in diglyme electrolyte than the in carbonate-based electrolyte. More stable cyclic performance is also obtained in diglyme electrolyte (Figure S2), proving the excellent stability of as-prepared HC. Owing to low voltage plateau of HC, its capacity is primarily affected by the interior resistance of the electrode and electrolyte. When the resistance increases, polarization will shift this plateau to a lower or even negative voltage, leading to an incomplete discharge process if the cut-off voltage is set at 0V. It signifies the importance of designing effective cell configuration and test conditions in evaluating the Na storage behaviors in HC. Nevertheless, glyme based electrolyte has some limitations on the cathode side,[28] the following studies focus on carbonate electrolyte but with a low current density.

The Na storage mechanism in HC has been controversial. A sloping curve below 1.0 V followed by a plateau at around 0.1 V is observed in the voltage profile. While the sloping one could be assigned to Na ion adsorption on the isolated graphene layers, the mechanism on the plateau region is due possibly to either Na intercalation between graphitic domains

or pore filling in the nanopores. Therefore, ex situ Raman test is conducted to investigate how Na ions are stored in the as-prepared HC. The spectra at different charge/discharge depths are collected. Figure 2c indicates that all of the Raman spectra show the D-band at ~1350 cm^{-1} and G-band at ~1600 cm^{-1} during the whole cycling processes without a clear shift of the positions. As reported before, intercalation of alkali metals into the graphitic structure would lead to the shifting and splitting of G-band. The observation rules out the Na ion intercalation into the graphitic layers. Instead, the pore filling of Na ions in the nanopores is responsible for the low voltage plateau for the HC produced in this study.
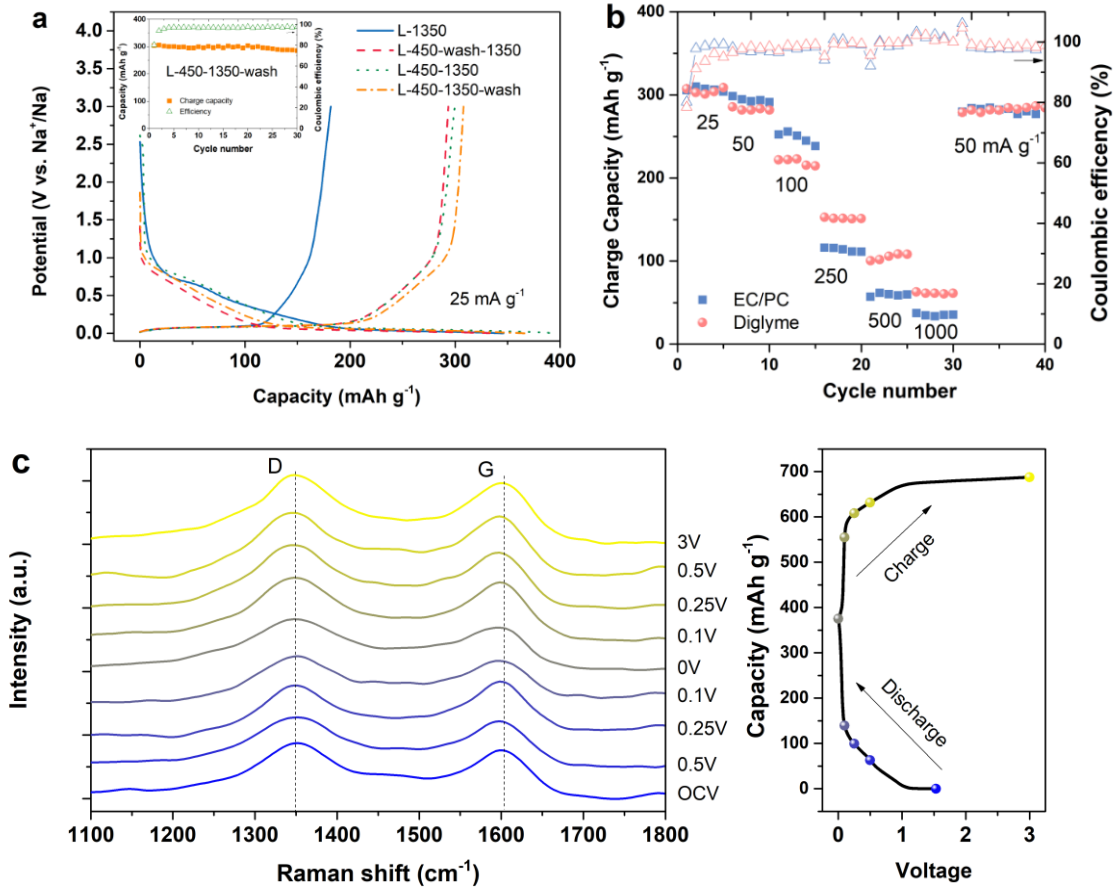

Figure 2 a) Galvanostatic charge/discharge curves and b) rate capabilities of HC half-cell. c) Ex situ Raman spectra of HC half cell.

The performance of HC was also evaluated at a low temperature of −20°C in half cell. A small current density of 10 mA g^{-1} was used for fully exploring its Na storage capability. It is not surprising that a capacity of less than 100 mAh g^{-1} is obtained with a 0 V cut-off

voltage due to the resistance drop. Therefore, the capacity limitation is used for low temperatures instead of voltage limitation, which may induce the Na plating on the electrode. In situ XRD is consequently conducted to monitor the phase evolution during prolonged discharge capacity. A Be-window equipped Swagelok cell was employed for the test, and the cell was pre-cycled to exclude the capacity contribution from SEI formation. Figure 3a shows the XRD patterns of HC discharged to the various status at −20°C. There is no noticeable change until the cell is discharged to 350 mAh g^{-1}, where a peak at around 42° corresponding to the Na (200) peak appears. Another peak at approximately 29.5° that attributed to Na (110) peak comes up when increasing the discharge capacity to 400 mAh g^{-1}. The intensity of the peak is enhanced with more Na plating at the sample discharged to 450 mAh g^{-1}. Once charging back to 3V, the Na (110) peak decreases but still exist, implying the low efficiency of Na plating/stripping. The plating of Na can also be examined from the voltage profiles. Two additional peaks at - 0.089 and 0.068 V, corresponding respectively to the plating and stripping of metallic Na, are observed in the dQ/dV curve for the cell testing at a cut-off capacity of 450 mAh g^{-1} as indicated in Figure S3d, and low Coulombic efficiency of 88.4% is obtained. One may still argue the accuracy of in situ XRD tests as the signal of metallic Na would not be detectable until the amount is accumulated to a specific value. In order to determine the Na plating capacity more punctually, ex situ XRD is conducted on HC electrodes in coin cells with capacity limitation from 200 to 300 mAh g^{-1}. The cells were cycled for 10 cycles to accumulate potential metallic Na. XRD patterns were collected at a discharged state. As shown in Figure S4, no Na peak is observed beneath the capacity of 250 mAh g^{-1}, and the Na signal appeared in 300 mAh g^{-1} sample. The Coulombic efficiency provides implications. The average Coulombic efficiency is around 97.4% for the cells cycling at a limited capacity of 250 mAh g^{-1} or less. The value is close to 97.8% when the cell is tested at room temperature with a cut-off voltage of 0 V. For the cell cycled at 300 mAh g^{-1}, the Coulombic efficiency decreases to only 95.3% due to the Na plating/stripping. Hence the capacity of 250 mAh g^{-1} is regarded as the reversible and safe capacity limitation for HC at -20°C.
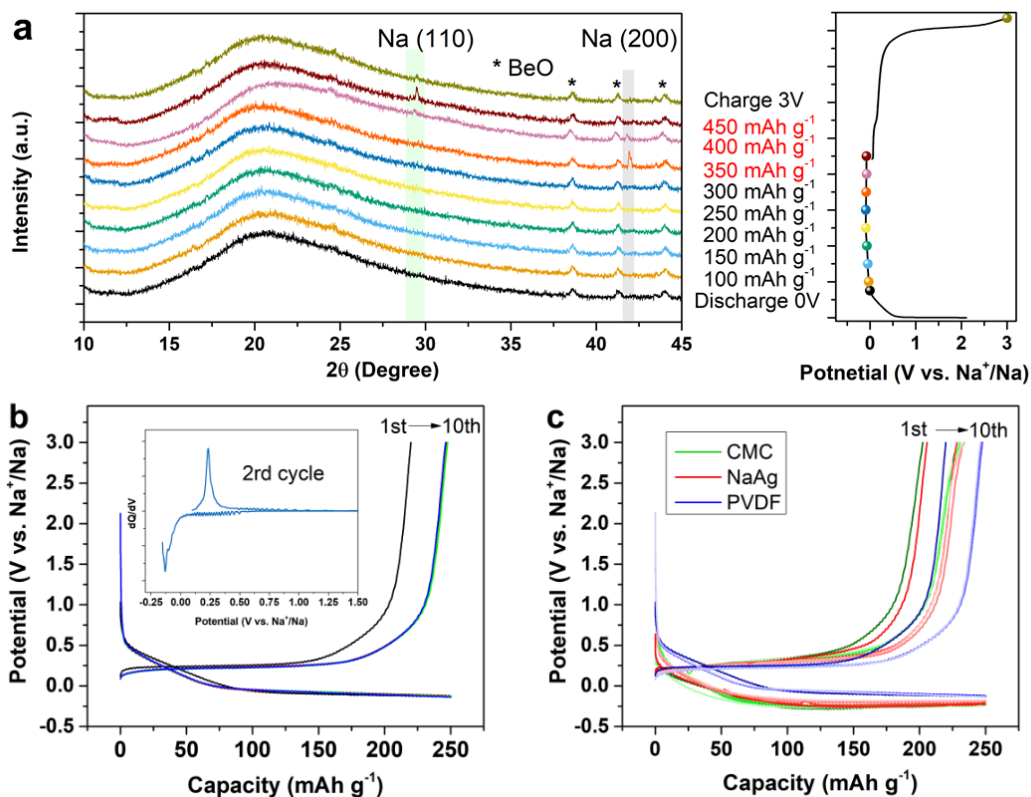
Figure 3a) In situ XRD pattern of HC cycled at −20°C. b) Voltage profiles of HC half-cell at −20°C with a capacity limitation of 250 mAh g^{-1}. c) Low-temperature performance of HC electrodes prepared with different binder materials.

Moreover, in situ Raman is adopted to investigate the ion storage behavior of HC at low temperature, and optical images were taken concomitantly. Figure S5 indicates no significant changes in Raman patterns during the entire discharge process, and the spectra are similar to that collected at 25°C, advocating the same sodium storage mechanism in HC at both low and room temperature. The optical images in Figure S6 clearly indicate the formation of Na metal at the capacity of 350 mAh g^{-1}. Sodium dendrite could be recognized at the capacity of 450 mAh g^{-1}. The above results suggest that sodium plating start to intervene around 300 mAh g^{-1}, and it will be safe to use HC within the capacity of 250 mAh g^{-1} at −20°C.

The performance of the electrode is not only affected by the active materials but also governed by the other components such as electrolyte and binder. It has been demonstrated

by Palacín et al. the importance of electrolyte formulation for the stable performance of HC at low temperature.[21] The binder plays a vital role in maintaining the structural integrity, but its effect under low temperature is not clear yet. Therefore, electrodes using several typical binders, including CMC, NaAg and PVDF are compared in Figure 3c for their low temperature performance. Among the three binders, PVDF exhibits the highest reversible capacity and the smallest resistance drop. This difference can be explained by the thermal stability of binder materials, as well-studied in Li-ion batteries.[29,30] To state in a simple way, PVDF has the lowest glass transition temperature (T_g) about −38 °C compared to CMC (121.7 °C) and NaAg (95.3 °C). For the operating temperature under −20 °C, CMC and NaAg become hard and brittle, making it difficult to retain the structural integrity of the active material in the electrode. Benefiting from its low T_g, the flexibility of PVDF is kept. Thus, PVDF is encouraged for practical application of NIB in a wide temperature range.

To provide a better understanding of the low-temperature performance of HC, we carried out a series of EIS analysis on the HC half-cell cycled at −20°C and 25°C. As revealed in Figure 4, the spectrum before cycling is composed of one small semicircle and a straight line, indicating the small impendence in the fresh cell. After cycling, a new semicircle at the high-frequency region is observed, particularly for cells at −20 °C. The high-frequency semicircle is associated with the resistance of SEI layer (Rsei), the middle-frequency semicircle is ascribed to the charge transfer resistance through the electrode/electrolyte interface (Rct), and the slope of the straight line in the low-frequency region refers to the diffusion condition of Na^+ ion in a solid-state compound. The value of Rsei, Rct and the resistance of the electrolyte (Rs) can be determined by fitting the equivalent circuit, and the results are listed in Table S1. Through the comparison, it is evident that both Rsei and Rct of cells cycled at −20 °C are ten times higher than cells at 25°C, revealing copious SEI is formed at low temperature and results in sluggish Na ion transfer. In addition, a stable SEI is built during the 1st charge/discharge cycle under room temperature, while the SEI continuously grew in the first 5 cycles at −20 °C. To further evaluate the SEI formed on the electrode surface, TEM characterizations of HC electrodes after 5 cycles under different temperature are showed in Figure 4c and 4d. The thickness

of SEI layer on HC surface is around 7 and 23 nm for electrode cycled at 25°C and −20°C, respectively, which is consistent with the EIS results confirming that a thicker SEI film would be formed at low temperature giving rise to higher resistance.
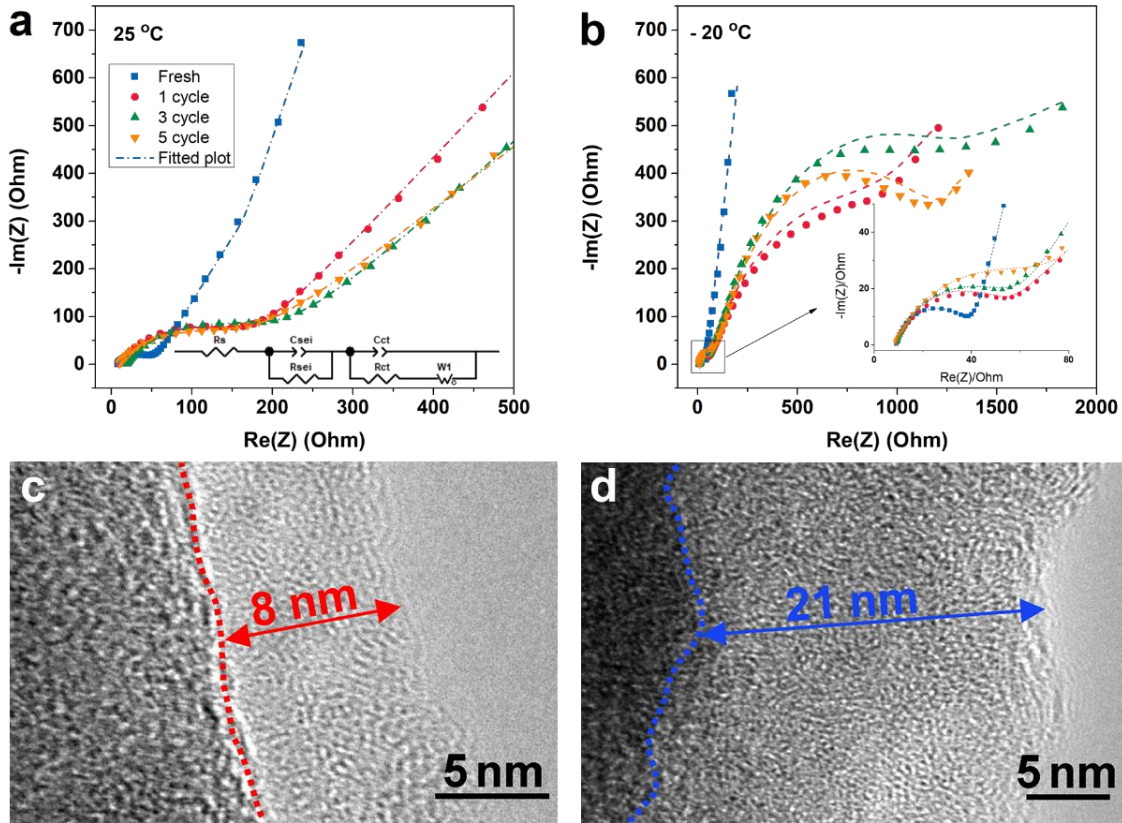

Figure 4 Nyquist plot of hard carbon half-cells at a) 25°C and b) -20°C, the dash lines represent the fitted plot from equivalent circuit. TEM images of hard carbon after cycling at c) 25 and d) −20 °C.

Performance of full cell using the HC electrode as the anode is then examined. A Na-rich $Na_{3.5}V_2(PO_4)_2F_3$ compound is utilized as the cathode. Compared to traditional $Na_3V_2(PO_4)_2F_3$, it is able to provide an additional 0.5 Na in the first cycle to compensate the Na consumed in SEI formation,[23] as shown in Figure 5a. The voltage profiles of $Na_{3.5}V_2(PO_4)_2F_3$/HC full cell consists of a plateau at 4.1 V and sloping regime between 3.6-2.5 V, contributing to an accumulative capacity of 306 mAh g^{-1} (based on the mass of anode). The energy density is calculated to be 310 Wh kg^{-1} based on the total weight of

13

cathode and anode, along with an average discharge potential of 3.62 V. A stable cyclic performance similar to that in half-cell is achieved at 25°C, as indicated by full cell F1 in Figure 5b.

Ulteriorly, we tested the behavior of full cell under low temperature. Firstly, the performance of $Na_{3.5}V_2(PO_4)_2F_3$ half-cell at 0°C and −20°C are measured and given in Figure S7a and S7b. The reversible capacity decreases with lowering the temperature. It maintains 93.2% and 80.4% of the capacity at room temperature for testing at 0°C and −20°C, respectively. Nevertheless, cyclic stability is kept. It is worthwhile to mention that the safe capacity for HC working at −20°C is 250 mAh g^{-1}, which is also around 80% of its capacity at room temperature. Therefore, there is no need to change the mass ratio of the cathode and anode in the full cell for operating at low temperature. As expected, the $Na_{3.5}V_2(PO_4)_2F_3$/HC full cell also demonstrates a capacity reduction at 0 °C in the first several cycles and reaches stable capacity retention of 244 mAh g^{-1} (F2 in Figure 5b). However, when the full cell was charged/discharged at −20°C, a significant drop in capacity is observed, particularly during the first 5 cycles. It may lie in the increased resistance on the anode side as reflected by EIS. The dynamic property of $Na_{3.5}V_2(PO_4)_2F_3$/HC at different temperatures is also evaluated using galvanostatic intermittent titration technique (GITT), as indicated in Figure 5c. From the calculation, the diffusion coefficient of Na-ions (D_{Na^+}) at 25°C is in the range of 10^{-9} to 10^{-10} cm^2 s^{-1}. The value is only slightly decreased at 0°C. In sharp contrast, the D_{Na^+} value is about one magnitude lower at −25 °C than that at 25°C. The slow Na^+ diffusion is in agreement with the EIS results that the thicker SEI film would affect the ion diffusion.

After testing at −20°C for 10 cycles, the same cell (F3) was put back to 25°C and its capacity gradually recovered and regained ca. 82% of the capacity at 25°C. It seems that the capacity of the full cell could not totally recover after cycling at low temperature. To figure out this matter, HC and $Na_{3.5}V_2(PO_4)_2F_3$ half-cells were investigated separately. As shown in Figure S8a, the capacity of both half cells is successfully restored to the value recorded at 25°C after 10 cycles at −20°C. It implies that the low temperature cycling affects neither the cathode nor the anode. The incapability of recovering the capacity may be ascribed to the consumption of Na at low temperature. Our previous discussion has shown that additional SEI is generated at −20 °C in the first five cycles, causing the

14

continuous consumption of Na. Half cells will not be much influenced as the excess Na anode is presented, but the full cell would be deteriorated as the available Na ions are fixed. To further confirm that the capacity loss is due to the Na consumption at low temperature, a full cell is tested at −20°C for only one cycle before taking back to room temperature (Figure S8b). 96% of the capacity is recovered compared to 82% for cycling at −20 °C for 10 cycles since less Na has been consumed in shorter cycles. In view of this finding, the challenge for the low temperature application of NIBs does not rely on the active materials. Instead, optimization on the electrolyte system is required in the future study to built a stable SEI.
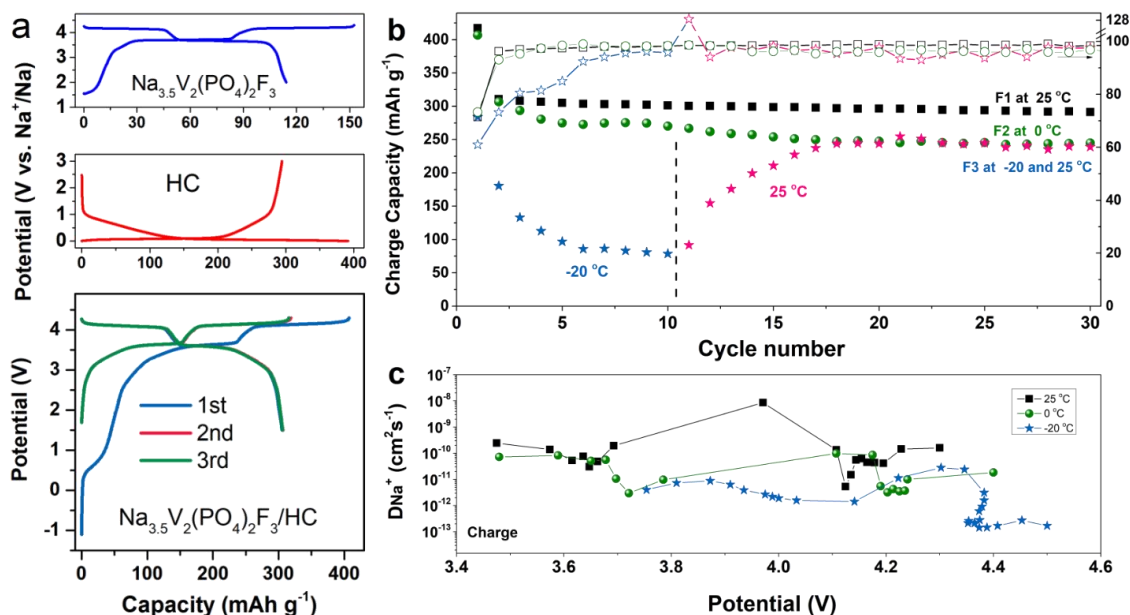

Fig. 5 Electrochemical performance of HC full cells with $Na_{3.5}V_2(PO_4)_2F_3$ cathode. a) Voltage profiles of $Na_{3.5}V_2(PO_4)_2F_3$, HC half cell and $Na_{3.5}V_2(PO_4)_2F_3$/HC full cell. b) Capacity retention and coulombic efficiency of full cells at −20°C, 0°C and 25°C. The capacity is calculated based on the weight of anode material. c) The diffusion coefficient of Na-ions (D_{Na}^+) calculated from GITT.

Conclusion

In summary, a hard carbon material for NIBs is fabricated from low-cost biomass waste using a facile two-step thermal treatment. Compared to direct high-temperature carbonization, the pre-treatment at a medium temperature is beneficial to avoiding the self-

activation effect of impurities. An appropriate surface area and pore size distribution are obtained, enabling a stable capacity of around 300 mAh g^{-1}. It also shows excellent performance at a temperature as low as −20 °C. A safe and reversible capacity of 250 mAh g^{-1} can be obtained without Na plating at −20 °C, as evidenced by in situ XRD and Raman tests. As-prepared HC also delivers stable performance in the full cell coupling with a $Na_{3.5}V_2(PO_4)_2F_3$ cathode, demonstrated an energy density of 310 Wh kg^{-1} (based on the total weight of electrode) with decent cyclic stability at room temperature. Nevertheless, the full cell shows a fast capacity fading at −20 °C due to both the increased resistance and continuous consumption of Na ions. It calls for building stable SEI under low temperature in future studies.

Acknowledgments

Reference

[1]   X. Wu, D. P. Leonard, X. Ji, *Chem. Mater.* **2017**, 29, 5031.

[2]   D. Kundu, E. Talaie, V. Duffort, L. F. Nazar, *Angew. Chemie Int. Ed*. **2015**, 54, 3431.

[3]   D. Larcher, J. Tarascon, *Nat. Chem.* **2014**, 7, 19.

[4]   E. Irisarri, A. Ponrouch, M. R. Palacin, *J. Electrochem. Soc.* **2015**, 162, A2476.

[5]   D. A. Stevens, J. R. Dahn, *J. Electrochem. Soc.* **2000**, 147, 1271.

[6]   E. Irisarri, N. Amini, S. Tennison, C. M. Ghimbeu, J. Gorka, C. Vix-Guterl, A. Ponrouch, M. R. Palacin, *J. Electrochem. Soc.* **2018**, 165, A4058.

[7]   E. M. Lotfabad, J. Ding, K. Cui, A. Kohandehghan, W. P. Kalisvaart, M. Hazelton, D. Mitlin, *ACS Nano* **2014**, 8, 7115.

[8]   C. Marino, J. Cabanero, M. Povia, C. Villevieille, *J. Electrochem. Soc.* **2018**, 165, A1400.

[9]   J. Ding, H. Wang, Z. Li, K. Cui, D. Karpuzov, X. Tan, A. Kohandehghan, D. Mitlin, *Energy Environ. Sci.* **2015**, 8, 941.

[10]   H. Wang, W. Yu, J. Shi, N. Mao, S. Chen, W. Liu, *Electrochim. Acta* **2016**, 188, 103.

[11]   P. Liu, Y. Li, Y. S. Hu, H. Li, L. Chen, X. Huang, *J. Mater. Chem. A* **2016**, 4, 13046.

[12]   Y. Qi, L. Mu, J. Zhao, Y. S. Hu, H. Liu, S. Dai, *Angew. Chemie Int. Ed.* **2015**, 54, 9911.

[13]   P. M. Bayley, N. M. Trease, C. P. Grey, *J. Am. Chem. Soc.* **2016**, 138, 1955.

[14]   X. Bi, X. Ren, Z. Huang, M. Yu, E. Kreidler, Y. Wu, *Chem. Commun.* **2015**, 51, 7665.

[15]   C. Ding, T. Nohira, R. Hagiwara, A. Fukunaga, S. Sakai, K. Nitta, *Electrochim. Acta* **2015**, 176, 344.

[16]   Q. Li, K. Jiang, X. Li, Y. Qiao, X. Zhang, P. He, S. Guo, H. Zhou, *Adv. Energy Mater.* **2018**, 8, 1801162.

[17]   M. Kang, Y. Wu, X. Huang, K. Zhou, Z. Huang, Z. Hong, *J. Mater. Chem. A* **2018**, 6, 22840.

[18]   Y.-Y. Wang, B. Hou, J. Guo, Q. Ning, W. Pang, J. Wang, C.-L. Lü, X.-L. Wu, *Adv. Energy Mater.* **2018**, 8, 1703252.

[19]   J.-Z. Guo, P. Wang, X. Wu, X.-H. Zhang, Q. Yan, H. Chen, J.-P. Zhang, Y.-G. Guo, *Adv. Mater.* **2017**, 29, 1701968.

[20]   D. A. Stevens, J. R. Dahn, *J. Electrochem. Soc.* **2001**, 148, A803.

[21]   A. Ponrouch, M. R. Palacín, *Electrochem. Commun.* **2015**, 54, 51.

[22]   C. Zhu, C. Wu, C. C. Chen, P. Kopold, P. A. Van Aken, J. Maier, Y. Yu, *Chem. Mater.* **2017**, 29, 5207.

[23]   B. Zhang, R. Dugas, G. Rousse, P. Rozier, A. M. Abakumov, J.-M. Tarascon, *Nat. Commun.* **2016**, 7, 10308.

[24]   S. Wanlapa, K. Wachirasiri, D. Sithisam-ang, T. Suwannatup, *Int. J. Food Prop.* **2015**, 18, 1306.

[25]   J. R. Dahn, W. Xing, Y. Gao, *Carbon* **1997**, 35, 825.

[26]   B. Zhang, C. M. Ghimbeu, C. Laberty, C. Vix-Guterl, J. M. Tarascon, *Adv. Energy Mater.* **2016**, 6, 1.

[27]   Y.-E. Zhu, L. Yang, X. Zhou, F. Li, J. Wei, Z. Zhou, *J. Mater. Chem. A* **2017**, 5, 9528.

[28]   K. Westman, R. Dugas, P. Jankowski, W. Wieczorek, G. Gachot, M. Morcrette, E. Irisarri, A. Ponrouch, M. R. Palacín, J.-M. Tarascon, P. Johansson, *ACS Appl. Energy Mater.* **2018**, 1, 2671.

[29]   H. Maleki, G. Deng, I. Kerzhner-Haller, A. Anani, J. N. Howard, *J. Electrochem. Soc.* **2000**, 147, 4470.

[30]   J.-P. Yen, C.-C. Chang, Y.-R. Lin, S.-T. Shen, J.-L. Hong, *J. Electrochem. Soc.* **2013**, 160, A1811.